https://doi.org/10.2352/EI.2024.36.7.ISS-286

Joint Design of Camera Spectral Sensitivity and Color Correction Matrix with Noise Consideration

Xinyue Yu, Masayuki Tanaka, Yusuke Monno, and Masatoshi Okutomi;
Tokyo Institute of Technology, Tokyo, Japan

Abstract

Camera spectral sensitivity (CSS) establishes the connection between scene radiance and device-captured RGB tristimulus values. Since the spectral sensitivity of most color imaging devices typically deviates from that of human vision or a standard color space and also noise is often introduced during the process of photoelectric signal conversion and transmission, the design of an efficient CSS with noise robustness and high color fidelity is of paramount importance. In this paper, we propose a CSS optimization method with noise consideration that designs theoretically an optimal CSS for each noise level. Additionally, taking practical considerations into account, we further extend the proposed method for a universally optimal CSS adaptable to diverse noise levels. Experimental results show that our optimized CSS is more robust to noise and has better imaging performance than existing optimization methods based on a fixed CSS. The source code is available at https://github.com/xyu12/Joint-Design-of-CSS-and-CCM-with-Noise-Consideration-EI2024.

Introduction

Camera spectral sensitivities (CSSs) are functions of wavelength describing the sensitivity of light detection for color filters and image sensors [1]. A digital color camera measures scene radiance as three primary pixel values: red, green, and blue (RGB) [2]. We refer to those measured RGB pixel values as camera RGB pixel values. The color space of device-dependent camera RGB is generally different from a standard sRGB color space [3, 4]. Therefore, we need to convert the camera RGB to the sRGB. This conversion is called color correction.

It is well-known that the performance of color reproduction via color correction strongly depends on the CSS. In [5, 6], the authors proposed an optimization algorithm of the CSSs assuming a noise-free situation, where the CSSs are optimized by minimizing the squared difference between estimated sRGB and true sRGB.

In practice, we need to take into account the effect of noise, because the measured pixel values include noise and it is amplified by the color correction process [7, 8]. There is a trade-off relationship between color reproduction performance and noise amplification. If we focus on the color reproduction performance only, the noise is severely amplified. Tan et al. introduced a metric that evaluates color reproduction performance by taking into account the noise amplification [9]. They also proposed a color correction method based on their metric. Gong et al. empirically showed that a broader CSS is more robust against noise but has lower color reproduction performance [10].

Inspired by those works [9, 10], we propose a CSS design method to improve color reproduction performance with the consideration of noise amplification. To simplify the problem, we assume a three-sensor case to avoid the effect of demosaicking in a single-sensor case with the Bayer color filter array [11].

In this paper, we first show an optimization method of the CSS for a certain noise level by minimizing the metric by Tan et al. [9]. Then, considering that it is infeasible to replace CSS for every noise level in practice, we also show an optimization method of the CSS for multiple noise levels. Experimental comparisons demonstrate that the CSS optimized by our method outperforms existing CSSs.

Preliminaries

The color of a pixel recorded by a digital camera depends on three physical factors: the spectral power distribution of the illuminant, the spectral reflectance of the object, and the CSS [6]. Consequently, the pixel value ρ can be modeled as

$$\rho_k = \int_\omega C_k(\lambda) S(\lambda) R(\lambda)\, d\lambda, \qquad k \in \{R,G,B\}, \tag{1}$$

where the subscript k denotes the color channel, λ indicates the wavelength defined on the visible spectrum ω (broadly speaking, 400nm to 700nm). The functions $C_k(\lambda)$, $S(\lambda)$, $R(\lambda)$ represent the CSS of the k-th color channel, the spectral distribution of the illuminant, and the spectral reflectance of the object, respectively.

For optimization, we consider a discrete version of Eq. 1 as

$$\rho_k = \boldsymbol{c}_k^T \cdot \boldsymbol{x}, \qquad k \in \{R,G,B\}, \tag{2}$$

where $\boldsymbol{x}$ is a discretized irradiance vector, $S(\lambda)R(\lambda)$, with a certain interval of the wavelength (10nm in our experiments), $\boldsymbol{c}_k$ is the corresponding discretized k-th CSS vector, and T represents the transpose operation.

We consider i.i.d. Gaussian noise [13] and use a simple linear color correction [14]. Let $\boldsymbol{X}$ be a matrix where each column contains the irradiance vector $\boldsymbol{x}$ of one pixel in the image and all the pixels are stacked in the column direction. Similarly, let $\boldsymbol{Q}$ be a matrix containing color-corrected sRGB values of all the pixels. Then, the estimated sRGB via color correction $\boldsymbol{Q}$ is written as

$$\boldsymbol{Q} = \boldsymbol{M}\left(\boldsymbol{C}^T\boldsymbol{X} + \boldsymbol{Z}\right), \tag{3}$$

where $\boldsymbol{C}$ is a CSS matrix containing the CSSs of three color channels, $\boldsymbol{Z}$ is an i.i.d. Gaussian noise matrix, and $\boldsymbol{M}$ is 3×3 color correction matrix (CCM).

Methodology

Figure 1 illustrates the overall imaging pipeline and the loss function for our optimization. Our optimization is a data-driven approach, where we utilize a dataset of hyperspectral images. We

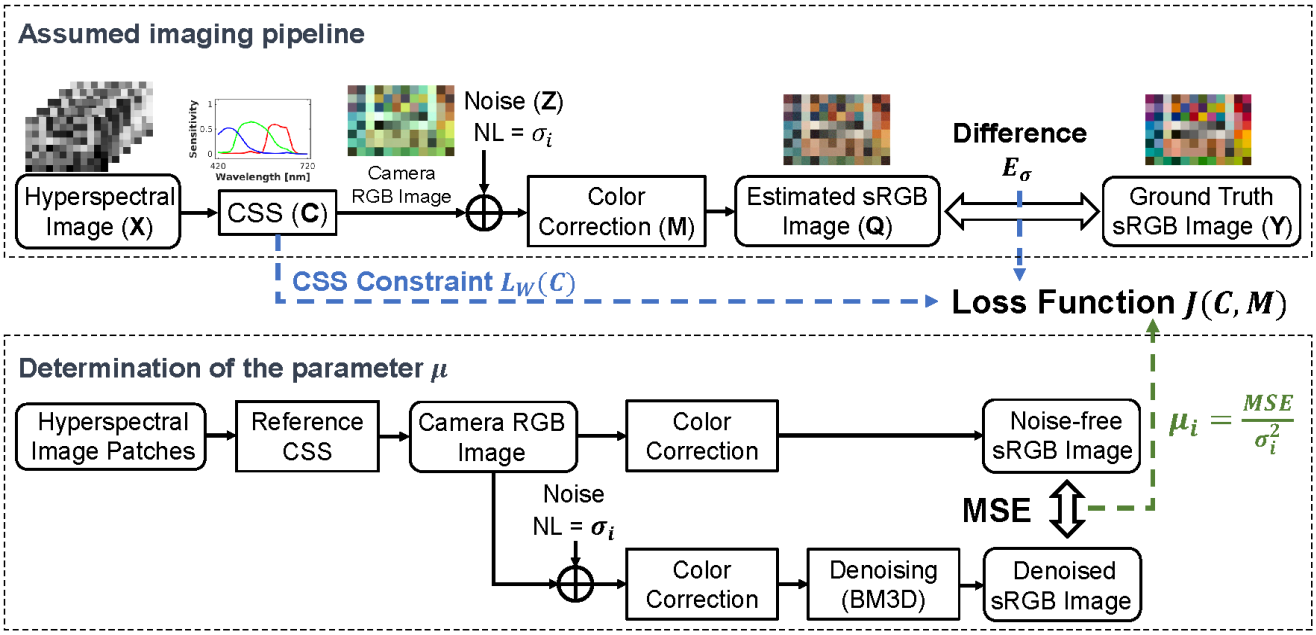

Figure 1. *The overall flow of our method for the joint design of camera spectral sensitivity and color correction matrix with noise consideration. The parameter μ is determined by assuming the BM3D denoising [12] in our proposed method.*

use the hyperspectral images as scene irradiance maps that are the products of lighting and reflectances. A camera RGB image is then obtained by multiplying an irradiance map with the CSS. After adding Gaussian noise, a CCM is applied to obtain the estimated sRGB image. Based on this pipeline, the CSS and the CCM are jointly optimized to minimize a loss function, which consists of two terms: the metric by Tan et al. [9], and a CSS constraint, which is a practical constraint of the CSS that the sensitivity of each wavelength should be within a specified value range. Furthermore, considering the final image reconstruction performance including denoising, we add the parameter μ to simulate the denoising effect in the optimization. This part will be explained in detail later.

In our method, we first introduce bias error and variance error based on the metric by Tan et al. [9]. Then, we simultaneously optimize the CSS matrix $\boldsymbol{C}$ and the CCM $\boldsymbol{M}$ for a certain noise level. Finally, we consider a multi-noise level case.

Assuming that there is no correlation between signal and noise, the metric by Tan et al. [9] can be expressed as

$$E_\sigma(\boldsymbol{C},\boldsymbol{M}) = \frac{1}{N}\|\boldsymbol{Q}-\boldsymbol{Y}\|_F^2 = \frac{1}{N}\|\boldsymbol{M}\left(\boldsymbol{C}^T\boldsymbol{X}\right)-\boldsymbol{Y}\|_F^2 + \sigma^2\|\boldsymbol{M}\|_F^2, \tag{4}$$

where $\boldsymbol{Y}$ is a matrix containing true sRGB values of a pixel in each column, N is the number of the pixels in the image, and σ is a noise level, i.e. a standard deviation of the noise. The first term in Eq. 4 of $\varepsilon_b = \frac{1}{N}\|\boldsymbol{M}\left(\boldsymbol{C}^T\boldsymbol{X}\right)-\boldsymbol{Y}\|_F^2$ represent a bias error. The second term of $\varepsilon_v = \sigma^2\|\boldsymbol{M}\|_F^2$ represent a variance error.

Individual optimization for single-noise-level case

Let σ be a given noise level. Here, we simultaneously optimize the CSS and the CCM for the given noise level. Before applying optimization, we need to consider a physical restriction of the CSS. Because the color filters are placed in front of the image sensor and block some parts of light, the resultant CSSs should not be beyond the sensitivity of the unfiltered monochrome image sensor, which is typically called white sensitivity [15]. Thus, we add this maximum sensitivity constraint to Eq. 4 as

$$J_\sigma(\boldsymbol{C},\boldsymbol{M}) = E_\sigma(\boldsymbol{C},\boldsymbol{M}) + L_W(\boldsymbol{C}), \tag{5}$$

where $L_W(\boldsymbol{C})$ represents what we call the white constraint of the CSS. This constraint is formulated as

$$L_W(\boldsymbol{C}) = \sum_{k,j}\ell_w(c_{kj}), \quad \ell_w(c_{kj}) = \begin{cases} 0, & 0 \le c_{kj} \le W_j \\ \infty, & else \end{cases}, \tag{6}$$

where k represents the color channel, j represents the index of the discrete wavelength, c_{kj} is the corresponding element of $\boldsymbol{C}$, and W_j is the spectral sensitivity of the unfiltered monochrome image sensor at the corresponding wavelength. This constraint gives an infinite cost if the element of the CSS, i.e., the sensitivity of each wavelength, is out of the range of $[0, W_j]$.

An optimal CSS depends on the noise level. Thus, in the first step, we jointly design an optimal CSS and CCM for a certain assumed noise level ($\sigma = 0, 2, 5, 8, 10, 20, 30$). In our experiments, the pixel values are normalized within the range $[0, 1]$, so the actual noise level needs to be divided by 255, respectively. Even though, for the sake of linguistic simplicity, we shall continue to express the noise level as described above in this paper. We jointly optimize the loss function in Eq. 5 regarding the CSS $\boldsymbol{C}$ and the CCM $\boldsymbol{M}$ by a proximal gradient descent (PGD) algorithm [16], given in the following Algorithm 1. As a result, we derive the optimal CSS and CCM corresponding to each distinct noise level.

Common optimization for multi-noise-level case

In pursuit of optimal image reconstruction performance, designing the CSS individually for each noise level is theoretically

Algorithm 1 PGD Algorithm for the Joint Optimization

Initialize $\boldsymbol{C}^0$ and $\boldsymbol{M}^0$ respectively with an existing CSS and an initial CCM obtained by least squares solution.
Notice that *iter* denotes the default value of iterations, and the $prox()$ function is employed to constrain the intensity of $\boldsymbol{C}^i$ within $L_W(\boldsymbol{C})$.
Learning rate of CSS and CCM are defined by lr_C and lr_M, as well as utilizing $grad_C$ and $grad_M$ to denote the gradient of Eq. 5 with respect to $\boldsymbol{C}$ and $\boldsymbol{M}$.
$\boldsymbol{C}^0 = Initial\ CSS, \boldsymbol{M}^0 = \boldsymbol{M}_{LS}, i = 0$, where $\boldsymbol{M}_{LS}$ is the least square solution of Eq. 5 for $\boldsymbol{C} = \boldsymbol{C}^0$.
while $i \leqslant iter$ **do**
    $\boldsymbol{C}^i = prox\left(\boldsymbol{C}^{i-1} - lr_C \times grad_C\right)$
    $\boldsymbol{M}^i = \boldsymbol{M}^{i-1} - lr_M \times grad_M$
    $i = i + 1$
end while
return $\boldsymbol{C}^i, \boldsymbol{M}^i$

advantageous. However, it is infeasible to change the CSS for each noise level in practice. Thus, we extend the previous section's approach to a multi-noise-level case.

Although we cannot easily change the CSS in hardware, we can easily change the CCM in software. Thus, we propose to optimize one CSS matrix $\boldsymbol{C}$ and multiple CCM $\boldsymbol{M}_{\boldsymbol{\sigma_i}}$ corresponding to the set of assumed noise levels. The loss function is denoted as

$$J(\boldsymbol{C}, \{\boldsymbol{M}_{\boldsymbol{\sigma_i}}\}) = \sum_{\sigma_i} E_{\sigma_i}(\boldsymbol{C}, \boldsymbol{M}_{\boldsymbol{\sigma_i}}) + L_W(\boldsymbol{C}), \tag{7}$$

which can be resolved using the *PGD* algorithm akin to that outlined in Algorithm 1. Consequently, this approach will yield one optimal CSS for all assumed noise levels along with optimal CCMs corresponding to each distinct noise level.

Joint optimization taking denoising into account

Currently, we have provided precise definitions for the loss functions in both optimization methods we described before. As defined in Eq. 4, we assign equal weight to the first term of bias error ε_b and the second term of variance error ε_v in the optimization process, which is in adherence to our proposed imaging pipeline. However, empirical experiments revealed that variance error predominantly influences optimization outcomes, which will result in the image reconstructed with our optimized CSS exhibiting a high signal-to-noise ratio but compromised color reconstruction quality, as elucidated in the subsequent section. This observation can be attributed to the absence of a denoising process within the assumed imaging pipeline. Nevertheless, conventional denoising algorithms often disrupt the linear transformation between the estimated sRGB values and the corresponding spectral radiance, thereby complicating the representation in the form of an optimization function. Consequently, we introduce a parameter μ to emulate the function of a denoising algorithm. With this parameter, Eq. 4 can be reformulated as

$$\hat{E}_\sigma = \varepsilon_b + \mu \cdot \varepsilon_v . \tag{8}$$

As illustrated in Fig. 1, to facilitate a more intuitive assessment of the imaging reconstruction quality of the aforementioned optimization methods, we employ the BM3D denoising algorithm [12]. We determine the parameter μ_i for varied noise levels by evaluating the error between noise-free and denoised images by utilizing hyperspectral image patches. The loss function and the optimization algorithms are the same as those discussed in the preceding sections except for the introduction of the parameter μ.

Experimental Results

Datasets and evaluation details

In our optimization, we require hyperspectral images or samples to form $\boldsymbol{X}$ in Eq. 4. For this purpose, we used the spectral reflectance data of 96 color patches of SG ColorChecker [17] and the CIE D65 illuminant. Consequently, the size of $\boldsymbol{X}$ becomes 31 by 96, where each column represents a 31-band irradiance vector for each color patch with the spectral range from 420nm to 720nm with intervals of 10nm.

Using the CSS and the CCM optimized with the 96 color checker samples, we evaluated their performance for two scenarios. The first evaluation was performed using the same 96 color checker samples, where the samples were rearranged to an image form with 100×100 pixels for each sample, as shown in Fig. 1. This is the ideal condition that the data used for optimization and testing are the same and thus can be used to confirm the theoretical correctness of our optimization. The second evaluation was performed using real hyperspectral images of the TokyoTech dataset [18]. The dataset contains a total of 30 scenes. We used the last 10 scenes for the evaluation and the remaining 20 scenes for estimating the parameter μ in the case including denoising. The second experiment can be used to confirm the robustness of our optimization for real-world scenarios.

Designed optimal CSSs

We selected the CSS of Sony IMX265 CMOS sensor (The CSS data were obtained from `https://thinklucid.com/`) shown in Fig. 2 (a) as an initial CSS for our optimization as well as the white constraint. We jointly designed the CSS and the CCM for the assumed noise levels. Figure 2 (b) shows the optimized CSSs in the single-noise-level case for the noise levels of 0, 10, and 30. We can observe that the CSSs for higher noise levels (e.g., 10 and 30) tend to be a broader shape. Figure 2 (c) shows the optimized CSS in the multi-noise-level case. From the results of both individual and common optimization methods, we can confirm that the shape of the CSS curves becomes wider to counteract the offset of the adverse effects of increased noise levels on image reconstruction quality.

Comparasions with other methods

The case without denoising. We compared our proposed methods with Tan et al. method [9] applied to existing Sony CSS. Tan et al. method only optimizes CCM for each noise level and does not change the CCS. For all the methods, we followed the imaging pipeline introduced in Fig. 1 to perform the color correction on the camera RGB image with added noise. To confirm the theoretical correctness of our optimization methods, we here excluded the denoising process and the parameter μ from the optimization process. Thus, the evaluation here was performed between resultant noisy sRGB images and ground-truth noise-free sRGB images.

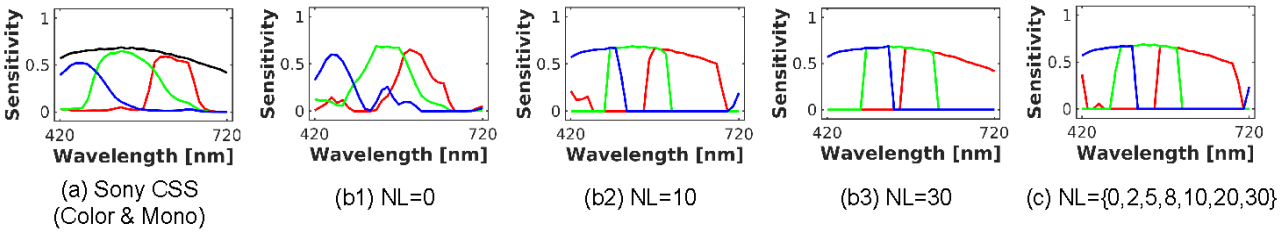

Figure 2. *Optimized CSSs using the 96 color patch samples of SG ColorChecker. (a) shows the initial Sony CSS. (b) shows the optimized CSSs by our individual optimization method for each noise level. (c) shows the optimized CSS by our common optimization method for multiple noise levels.*

Table 1: Numerical comparisons on SG ColorChecker dataset, where Individual (wo) and Common (wo) respectively denote the individual optimization and the common optimization methods without utilizing parameter μ and denoising.

Metric	Noise level	Sony CSS	Individual (wo)	Common (wo)
CPSNR	0	35.45	**45.86**	33.80
	2	34.34	**39.70**	33.44
	5	31.03	**33.69**	31.93
	8	28.19	**30.50**	30.09
	10	26.70	**29.05**	28.94
	20	22.13	**24.82**	24.65
	30	19.77	**22.41**	22.08
	Avg.	28.23	**32.29**	29.28
TPSNR	0	35.45	**45.86**	33.80
	2	34.34	**39.70**	33.44
	5	31.03	**33.69**	31.93
	8	28.19	**30.50**	30.09
	10	26.70	**29.05**	28.94
	20	22.13	**24.82**	24.65
	30	19.77	**22.41**	22.08
	Avg.	28.23	**32.29**	29.28

Table 2: Numerical comparisons on TokyoTech dataset, where Individual (wo) and Common (wo) respectively denote the individual optimization and common optimization methods without utilizing parameter μ and denoising.

Metric	Noise level	Sony CSS	Individual (wo)	Common (wo)
CPSNR	0	37.46	**48.27**	32.70
	2	34.94	**39.72**	31.67
	5	30.76	**33.37**	29.61
	8	27.84	**29.57**	27.92
	10	26.38	**27.77**	26.98
	20	22.09	23.27	**23.65**
	30	20.06	21.53	**21.62**
	Avg.	28.51	**31.93**	27.74
TPSNR	0	37.46	**48.27**	32.70
	2	34.94	**39.73**	31.68
	5	30.77	**33.38**	29.61
	8	27.85	**29.58**	27.93
	10	26.39	**27.78**	26.99
	20	22.10	23.27	**23.66**
	30	20.06	21.53	**21.63**
	Avg.	28.51	**31.93**	27.74

We used color peak signal-to-noise ratio (CPSNR) and theoretical peak signal-to-noise ratio (TPSNR) to evaluate the final image reconstruction performance of different methods. TPSNR is calculated as

$$TPSNR = 10 \times \log_{10}\left(\frac{1}{E_\sigma/3}\right), \tag{9}$$

where E_σ is calculated by Eq. 4 given the CSS and the CCM. TPSNR represents theoretically/computationally derived PSNR for the evaluated scenes.

Table 1 and 2 summarize the numerical comparisons on the SG ColorChecker dataset and the TokyoTech dataset, respectively. Both CPSNR and TPSNR metrics represent higher is better. Table 1 shows the results for SG ColorChecker data and shows that the proposed individual optimization method significantly outperforms the method by Tan et al. with Sony CSS at each noise level. The proposed common optimization method that designs a universally optimal CSS for multiple noise levels also performs much better than the baseline Sony CSS in the cases of high noise levels. Notice that the individual optimization method independently designs CSS and CCM for each noise level, thus it naturally achieves the best performance for the evaluation using SG ColorChecker. Meanwhile, the more practically meaningful common optimization method also outperforms the baseline, proving the superiority of our method.

Table 2 shows the results for the TokyoTech dataset and shows similar trends to Table 1. Specifically, under conditions of elevated noise levels exceeding 20, the common optimization demonstrates superior imaging performance in comparison to the individual optimization, emphasizing the role of our optimization function in improving the robustness for real-world scenarios.

In Table 1 and 2, it can be distinctly observed that CPSNR and TPSNR are nearly equal under identical optimization conditions. This observation underscores the efficacy of the mathematical models we have proposed, as they exhibit a robust fit to the imaging pipeline we have presented, even when applied to relatively small 96-patch data for optimization.

Figure 3 visually compares the output noisy sRGB images. In both Fig. 3 (a) and (b), the top row shows the output sRGB images and the bottom row shows the RMSE maps compared with the ground truth. The darker the color of the RMSE map, the lower the error between the output and ground-truth images.

In Fig. 3 (a), owing to the homogeneous color distribution and straightforward structure of the test image, superior image reconstruction quality is readily attainable. Our proposed methods conspicuously surpass the baseline in visual performance. Con-

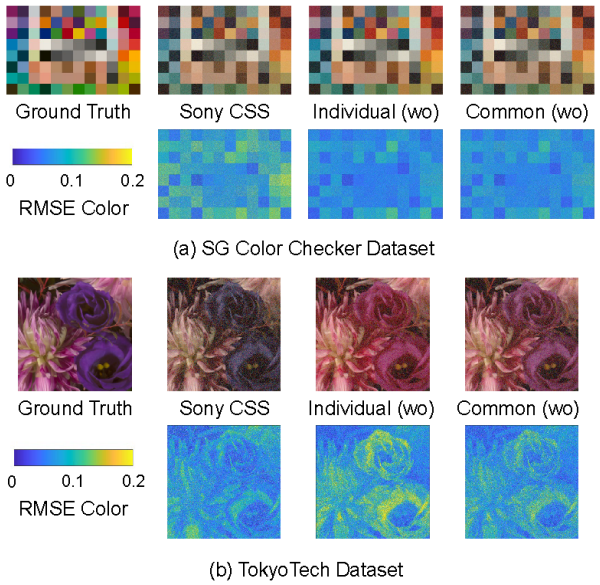

Figure 3. *Visual comparisons and RMSE maps of noisy sRGB images without including denoising and utilizing μ (wo), where the noise level is 30.*

trastingly, in Fig. 3 (b), given the comparatively intricate color distribution in the TokyoTech dataset, our optimization outcomes exhibit inaccuracies in reproducing image color, even when confronted with a high signal-to-noise ratio. Considering that there exists a trade-off between noise robustness and color reconstruction performance during the CSS optimization process, a broader CSS is more robust against noise but has lower color reproduction. In the interim, it is well-established that the color correction process amplifies image noise, thereby accentuating the predominant influence of the variance error defined in Eq. 4 during joint optimization. In light of the confluence of these influencing factors, it proves challenging for the optimization method we have introduced to ensure the color reconstruction quality of the image under conditions of elevated noise levels, notwithstanding its comparative superiority over the baseline.

The case with denoising. Motivated by the suboptimal performance observed in color reconstruction in the preceding section, it became evident that, throughout the optimization procedure, the variance error ε_v assumes a dominant role, exhibiting magnitudes dozens of times larger than the bias error ε_b, thus we employed the parameter μ to properly weight these two error terms.

Table 3 and 4 summarize the numerical comparisons of the denoised images on the two different datasets. It can be markedly observed that, after taking the denoising factor into account, our optimization method is significantly superior to the baseline. In high noise level cases, the common optimization method has distinct advantages. While the common optimization method lags behind the individual optimization in low-noise-level conditions, its emphasis on designing a CSS adaptable to multiple noise levels has proven its superior imaging reconstruction performance in practical scenarios. Notably, across various noise stages, it outperforms the Tan et al. method, which only optimizes the CCM with noise consideration while utilizing a fixed Sony CSS.

Table 3: Numerical comparisons on SG ColorChecker dataset, where Individual (w) and Common (w) respectively denote the individual optimization and the common optimization methods with parameter μ utilized and denoising included.

Metric	Noise level	Sony CSS	Individual (w)	Common (w)
CPSNR	0	35.45	**45.86**	39.92
	2	35.43	**45.41**	39.91
	5	35.17	**44.04**	39.84
	8	34.20	**42.33**	39.67
	10	33.13	**41.18**	39.50
	20	27.46	35.90	**37.70**
	30	23.96	32.91	**35.05**
	Avg.	32.11	**41.09**	38.80

Table 4: Numerical comparisons on TokyoTech dataset, where Individual (w) and Common (w) respectively denote the individual optimization and common optimization methods with parameter μ utilized and denoising included.

Metric	Noise level	Sony CSS	Individual (w)	Common (w)
CPSNR	0	37.46	**48.27**	40.35
	2	36.20	**43.08**	38.59
	5	34.68	**39.45**	36.82
	8	33.37	**37.33**	35.66
	10	32.43	**36.26**	35.07
	20	28.05	31.29	**32.88**
	30	25.40	28.33	**31.16**
	Avg.	32.51	**37.71**	35.79

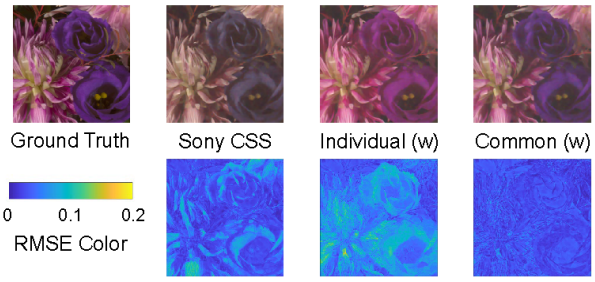

Figure 4. *Visual comparisons and RMSE maps of denoised images with the parameter μ utilized (w), where noise level is* 30

The outstanding performance of the common optimization method in color reconstruction can be illustrated sufficiently in Fig. 4. Through the visual comparison, it becomes evident that the proposed common optimization method significantly outperforms other methods, especially in high-noise-level cases.

Conclusion

In this paper, we have proposed a method to derive a theoretically optimal CSS. We have first introduced an individual optimization method for jointly designing CSS and CCM in single-noise-level cases. Additionally, taking practical considerations

into account, we further have extended the method to derive a commonly optimal CSS for the multi-noise-level case. Simultaneously, considering the color reproduction performance of the optimized CSS, we have incorporated a weighting parameter μ into the optimization function, simulating the denoising algorithm's role in the assumed imaging pipeline. Experimental comparisons have demonstrated that the CSSs optimized by our methods outperform existing CSSs among a wide range of noise levels.

References

[1] Jun Jiang, Dengyu Liu, Jinwei Gu, and Sabine Süsstrunk, "What is the space of spectral sensitivity functions for digital color cameras?," in *IEEE Workshop on Applications of Computer Vision (WACV)*, 2013, pp. 168–179.

[2] Seonghyeon Nam, Abhijith Punnappurath, Marcus A Brubaker, and Michael S Brown, "Learning sRGB-to-raw-RGB de-rendering with content-aware metadata," in *IEEE/CVF Conference on Computer Vision and Pattern Recognition (CVPR)*, 2022, pp. 17704–17713.

[3] Noboru Ohta and Alan Robertson, *Colorimetry: Fundamentals and applications*, John Wiley & Sons, 2006.

[4] Graham Finlayson, Yuteng Zhu, and Han Gong, "Using a simple colour pre-filter to make cameras more colorimetric," in *Color Imaging Conference (CIC)*, 2018, pp. 182–186.

[5] Gaurav Sharma and H Joel Trussell, "Figures of merit for color scanners," *IEEE Transactions on Image Processing*, vol. 6, no. 7, pp. 990–1001, 1997.

[6] Graham Finlayson and Yuteng Zhu, "Designing color filters that make cameras more colorimetric," *IEEE Transactions on Image Processing*, vol. 30, pp. 853–867, 2020.

[7] Kenta Takahashi, Yusuke Monno, Masayuki Tanaka, and Masatoshi Okutomi, "Effective color correction pipeline for a noisy image," in *IEEE International Conference on Image Processing (ICIP)*, 2016, pp. 4002–4006.

[8] Ryo Yamakabe, Yusuke Monno, Masayuki Tanaka, and Masatoshi Okutomi, "Tunable color correction for noisy images," *Journal of Electronic Imaging*, vol. 29, no. 3, pp. 033012–1–24, 2020.

[9] Yap-Peng Tan and Tinku Acharya, "Method for color correction with noise consideration," in *Proc. of SPIE*, 1999, vol. 3963, pp. 329–337.

[10] Zilai Gong, Masayuki Tanaka, Yusuke Monno, and Masatoshi Okutomi, "Optimal noise-aware imaging with switchable prefilters," in *IEEE International Conference on Image Processing (ICIP)*, 2022, pp. 2771–2775.

[11] Bryce Bayer, "Color imaging array," *United States Patent, no. 3971065*, 1976.

[12] Kostadin Dabov, Alessandro Foi, Vladimir Katkovnik, and Karen Egiazarian, "Image denoising by sparse 3-D transform-domain collaborative filtering," *IEEE Transactions on Image Processing*, vol. 16, no. 8, pp. 2080–2095, 2007.

[13] Ali Maleky, Shayan Kousha, Michael S Brown, and Marcus A Brubaker, "Noise2NoiseFlow: Realistic camera noise modeling without clean images," in *IEEE/CVF Conference on Computer Vision and Pattern Recognition (CVPR)*, 2022, pp. 17632–17641.

[14] Graham Finlayson, Maryam Mohammadzadeh Darrodi, and Michal Mackiewicz, "The alternating least squares technique for nonuniform intensity color correction," *Color Research & Application*, vol. 40, no. 3, pp. 232–242, 2015.

[15] Ayan Chakrabarti, William T Freeman, and Todd Zickler, "Rethinking color cameras," in *IEEE International Conference on Computational Photography (ICCP)*, 2014, pp. 1–8.

[16] Takashi Shibata, Masayuki Tanaka, and Masatoshi Okutomi, "Gradient-domain image reconstruction framework with intensity-range and base-structure constraints," in *IEEE Conference on Computer Vision and Pattern Recognition (CVPR)*, 2016, pp. 2745–2753.

[17] Yusuke Monno, Hayato Teranaka, Kazunori Yoshizaki, Masayuki Tanaka, and Masatoshi Okutomi, "Single-sensor RGB-NIR imaging: High-quality system design and prototype implementation," *IEEE Sensors Journal*, vol. 19, no. 2, pp. 497–507, 2018.

[18] Yusuke Monno, Sunao Kikuchi, Masayuki Tanaka, and Masatoshi Okutomi, "A practical one-shot multispectral imaging system using a single image sensor," *IEEE Transactions on Image Processing*, vol. 24, no. 10, pp. 3048–3059, 2015.

Author Biography

Xinyue Yu is a master's student from Okutomi and Tanaka Laboratory, Tokyo Institute of Technology. Her research interests include image signal processing and image recognition. She received her bachelor's degree in Auto Body Engineering from Jilin University, China in 2020.

Masayuki Tanaka received his Ph.D. degree from Tokyo Institute of Technology in 2003. He was an Associate Professor at the Graduate School of Science and Engineering, Tokyo Institute of Technology, from 2008 to 2016. He was a Visiting Scholar at Stanford University, from 2013 to 2014. He was an Associate Professor at Tokyo Institute of Technology, from 2016 to 2017. He was a Senior Researcher at National Institute of Advanced Industrial Science and Technology, from 2017 to 2020. He was an Associate Professor at Tokyo Institute of Technology, from 2020 to 2023. Since 2023, he has been a Professor at Tokyo Institute of Technology.

Yusuke Monno received the B.E., M.E., and Ph.D degrees from Tokyo Institute of Technology, Tokyo, Japan, in 2010, 2011, and 2014, respectively. He is currently a specially appointed associate professor with the Department of Systems and Control Engineering, School of Engineering, Tokyo Institute of Technology. He received various awards including the ICIP Best Student Paper Award in 2022. His research interests are in both theoretical and practical aspects of image processing and computer vision.

Masatoshi Okutomi received his master's degree from Tokyo Institute of Technology in 1983 and joined Canon Inc., Tokyo, Japan. He was a visiting research scientist at Carnegie Mellon University, PA, USA from 1987 to 1990. He received his Ph.D. degree from Tokyo Institute of Technology in 1993. He is currently a Professor at Tokyo Institute of Technology.